








The effect of root hairs on root water uptake is determined by root–soil contact and root hair shrinkage

Patrick Duddek¹ , Mutez Ali Ahmed² , Mathieu Javaux³ , Jan Vanderborgh³ , Goran Lovric⁴ ,
Andrew King⁵  and Andrea Carminati¹ 

¹Department of Environmental Systems Science, Physics of Soils and Terrestrial Ecosystems, Institute of Terrestrial Ecosystems, ETH Zürich, Universitätsstrasse 16, 8092, Zurich, Switzerland;

²Root-Soil Interactions, School of Life Sciences, Technical University of Munich, D-85354, Freising, Germany; ³Agrosphere Institute, IBG-3, Forschungszentrum Jülich GmbH, 52425,

Jülich, Germany; ⁴Swiss Light Source, Paul Scherrer Institute, Forschungsstrasse 111, 5232, Villigen, Switzerland; ⁵Synchrotron SOLEIL, L'Orme des Merisiers, 91192, Gif-sur-Yvette Cedex, France

Summary

Author for correspondence:

Patrick Duddek

Email: patrick.duddek@usys.ethz.ch

Received: 24 May 2023

Accepted: 29 June 2023

New Phytologist (2023)

doi: 10.1111/nph.19144

Key words: capillary barrier, drought stress, hydraulic conductivity, image-based modelling, pore-scale, root hairs, root water uptake, root–soil contact.

- The effect of root hairs on water uptake remains controversial. In particular, the key root hair and soil parameters that determine their importance have been elusive.
- We grew maize plants (*Zea mays*) in microcosms and scanned them using synchrotron-based X-ray computed microtomography. By means of image-based modelling, we investigated the parameters determining the effectiveness of root hairs in root water uptake. We explicitly accounted for rhizosphere features (e.g. root–soil contact and pore structure) and took root hair shrinkage of dehydrated root hairs into consideration.
- Our model suggests that > 85% of the variance in root water uptake is explained by the hair-induced increase in root–soil contact. In dry soil conditions, root hair shrinkage reduces the impact of hairs substantially.
- We conclude that the effectiveness of root hairs on root water uptake is determined by the hair-induced increase in root–soil contact and root hair shrinkage. Although the latter clearly reduces the effect of hairs on water uptake, our model still indicated facilitation of water uptake by root hairs at soil matric potentials from -1 to -0.1 MPa. Our findings provide new avenues towards a mechanistic understanding of the role of root hairs on water uptake.

Introduction

Plant growth and productivity are strongly influenced by environmental stresses such as nutrient and water scarcity. In many places around the world, the acquisition of the respective soil resources by plants will be severely impeded in the near future as a consequence of climate change. As root hairs are considered to be a key rhizosphere trait with the potential to enhance plant ability to capture soil resources, they are advocated as a breeding target for developing more stress-resilient crops (White & Kirkegaard, 2010; Brown *et al.*, 2013; Zhang *et al.*, 2018; Marin *et al.*, 2021).

Root hairs, cylindrical extensions of epidermal root cells, provide multiple benefits for plants, while the carbon costs of these single-cell structures are relatively low (Hetrick, 1991; Bates & Lynch, 2001). By substantially increasing root surface area and root–soil contact (Gahoonia & Nielsen, 1997; Haling *et al.*, 2013; Duddek *et al.*, 2022), they enlarge the root absorptive surface available for the acquisition of soil resources. As they can access finer pores than the main root axis, they further increase the volume of soil affected by roots (Tisdall, 1991). Hence, they are hypothesised to facilitate both nutrient and water uptake, especially in drying soil. Their pivotal role in the uptake of

immobile nutrients, such as phosphorus, is well accepted (Bates & Lynch, 2001; Gahoonia & Nielsen, 2003; Haling *et al.*, 2013; Keyes *et al.*, 2013). In contrast, the role of root hairs in root water uptake remains controversial. Utilising a micropotometer, Cailloux (1972) showed that root hairs of oats have the ability to absorb water. As the total amount of absorbed water was considerably greater than the quantity required for root hair growth, the author concluded that the excess water contributed to root water uptake. More recent studies focussed on comparing root hair defective mutants with their corresponding wild-types. Considering various plant species and environmental conditions, experimental approaches in both laboratory and field trials have yielded contradictory results. By measuring the transpiration rate of rice plants under increasing water stress, Suzuki *et al.* (2003) found that, at the seedling stage, root hairs did not contribute to root water uptake. Similarly, in barley, Li *et al.* (2014) found that root hairs did not enhance plant drought tolerance. This was confirmed by Dodd *et al.* (2016) who did not find differences in transpiration rate and leaf water potential between a root hair defective mutant (*brb*) and the corresponding wild-type. The authors suggested that the mutant may have compensated for the lack of root hairs by developing larger root systems.

Furthermore, they argued that root hairs may only become important at high transpiration rates. Indeed, investigating the same barley genotypes, Carminati *et al.* (2017) found that the wild-type was able to sustain higher transpiration rates under dry soil conditions compared with the mutant. The authors suggested that the uptake of water by root hairs diverts the flow from within the soil into root hairs which, under high transpiration rates, results in smaller matric potential gradients and hence in a lower reduction in hydraulic conductivity at the root–soil interface.

Similar results were found by Marin *et al.* (2021) in the framework of a field experiment. In total, five barley genotypes exhibiting different root hair lengths and densities were grown in two soil textures (sandy loam and clay loam). Climatic conditions between the two growing seasons differed substantially. Under wet conditions, root hairs had no significant effect on plant water status. However, under water-deficient conditions, hairy genotypes exhibited less negative leaf water potentials and lower leaf abscisic acid concentration. Surprisingly, in a comparable field experiment with maize, root hairs did not confer a significant effect on plant water uptake (Jorda *et al.*, 2022). Again, a root hair defective mutant (*rth3*) and the corresponding wild-type were grown in two contrasting soil textures (loam and sand). Both soil and plant data were interpreted using a mechanistic root water uptake model (Cai *et al.*, 2018). The transpiration rate of the mutant was not reduced at less negative soil water potentials compared with the wild-type. The root systems of both genotypes extracted the entire plant available water in both soil textures, and there was no direct evidence of root hairs ameliorating root water uptake. Cai *et al.* (2021) investigated the same maize genotypes by applying the plant pressure method (Pasioura, 1980; Carminati *et al.*, 2017). In line with Jorda *et al.* (2022) but contradicting with Carminati *et al.* (2017), the authors found that root hairs had only a minor, if any, contribution to soil–plant hydraulics. They concluded that the role of root hairs in water uptake might be both species and soil specific.

Complementary to these experimental studies, various approaches and concepts have been developed to mathematically model root water uptake. In the pioneering work of Gardner (1960), water flow from bulk soil towards the root surface was computed by solving the Richardson–Richards equation analytically. This microscopic one-dimensional model was based on the assumption of a cylindrical root as a constant flux boundary, while the hydraulic properties of the rhizosphere were not distinguished from those of the bulk soil. Root hairs were considered in the model of Segal *et al.* (2008) who solved the Richardson–Richards equation on an artificial 2D biological-hydraulic geometry comprising a cylindrical root and multiple parallel root hairs. They found that the matric potential of the inter-root hair domain quickly reached the value prevalent in the root. This led the authors to conclude that mass flow in this region is limited and root hairs do not increase root water uptake by increasing root surface area. Instead, they argued that root hairs absorb water exclusively at their tip planes and function in water uptake by increasing the effective root diameter. However, this model is based on continuum equations, which suggests that the rhizosphere and its contrasting hydraulic properties relative to the bulk soil were neglected. In particular, the authors did not

account for the augmented porosity at the root–soil interface (Helliwell *et al.*, 2017; Landl *et al.*, 2021), which implies that root hairs rather bridge gaps between the root cylinder and the soil matrix (White & Kirkegaard, 2010; Robbins & Dinneny, 2015). This may change the evolution of matric potential gradients within the immediate vicinity of the root.

Three-dimensional (image-based) root system architecture models have also been developed, calculating water flow in the soil and root domains numerically (Doussan *et al.*, 1998; Dunbabin *et al.*, 2006; Javaux *et al.*, 2008; Daly *et al.*, 2018; Schnepf *et al.*, 2018). Some of the aforementioned modelling approaches do not discriminate between bulk soil and rhizosphere. Yet, since the contrasting hydraulic properties between those soil regions have been well recognised (Lavelle, 2002; Gregory, 2006; Watt *et al.*, 2006; Hinsinger *et al.*, 2009; Carminati *et al.*, 2010), the influence of rhizosphere traits on root water uptake is attracting growing attention. For example, Couvreur *et al.* (2014) accounted for the impact of changing root–soil contact with soil drying by changing the radial root hydraulic conductance as a function of the soil water content. Using a continuum approach, de Willigen *et al.* (2018) evaluated the impact of nonuniform root–soil interactions on root water uptake using analytical solutions for a cylindrical root. They found that the effect of partial radial root–soil contact was low. However, considering a loamy soil, they found that partial longitudinal root–soil contact exhibited a considerable effect on water uptake: A root–soil contact fraction of *c.* 5% reduced the duration of potential uptake by 50%. Nevertheless, the geometrical complexity of root–soil contact and its impact on root water uptake increases when root hairs and soil aggregates are taken into account. Due to the lack of spatial resolution and image contrast, resolving rhizosphere features has not been possible in previous studies. However, advances in synchrotron radiation X-ray CT have been particularly helpful, providing unprecedented spatial and temporal resolution and allowing the generation of pore-scale models that explicitly account for rhizosphere traits and soil structure. The combination of synchrotron radiation-based imaging and image-based modelling in the field of root–soil interactions was introduced by Aravena *et al.* (2011), who studied the influence of root-induced soil compaction on rhizosphere water flow and uptake by roots. Since then, a variety of image-based models have been developed for investigating processes like nutrient movement in the rhizosphere and uptake by roots (Keyes *et al.*, 2013; Daly *et al.*, 2016; Koebernick *et al.*, 2017) or carbon diffusion from roots and root hairs into the rhizosphere (Schnepf *et al.*, 2022). Although computationally highly demanding, these detailed and explicit models can be utilised to parameterise, test and validate upscaled and less complex models (Roose *et al.*, 2016).

To our knowledge, water uptake of root hairs has never been simulated in a systematic way at the appropriate scale, taking spatial rhizosphere heterogeneities and variations in root hair length and density into account. We aim to close this knowledge gap by combining synchrotron radiation X-ray CT, image processing and image-based modelling. Simulations of this study were carried out on root segments of maize (*Zea mays*) grown in a loamy soil.

Our objective was to identify the environmental conditions (e.g. soil water content) and hair traits (e.g. length, density and shrinkage point) that determine the importance of root hairs in water uptake.

Materials and Methods

The approach taken in this study can be summarised as follows (detailed description below). Under controlled conditions, we grew maize (*Zea mays* L.) plants in microcosms consisting of seedling holders and plastic cylinders, both filled with a loamy soil. After 14 d of growth, we harvested the plants and scanned individual plastic cylinders containing both soil and roots using synchrotron radiation-based X-ray CT. The collected images were used to extract three-dimensional geometries of roots, root hairs and soil matrix by means of image processing (Duddek *et al.*, 2022). Based on these extracted geometries, we simulated root water uptake by numerically solving the Richardson–Richards equation for a variety of scenarios (see Eqn 4). The simulations were performed before and after digital removal of root hairs from the root cylinders. We also included root hair shrinkage in additional simulations to estimate its effect on water uptake.

Our approach allowed us to focus on the effect of geometric aspects of both root hairs and the root–soil interface on water uptake, while minimising the number of variables that would be introduced by analysing a root hair defective mutant and the corresponding wild-type.

We would like to emphasise that our simulations were not intended to mimic the water flow conditions that prevailed during the scanning process. Instead, we used the collected image data to extract the required geometrical information, which allowed us to estimate the role of root hairs in water uptake under general conditions.

Plant growth

Maize (*Z. mays*) seeds were pregerminated on filter paper for 48 h before being placed individually into 3D-printed microcosms (Keyes *et al.*, 2013). The microcosms comprised seven 1.3 ml plastic cylinders (80 mm length, 4.5 mm inner diameter) that were connected to a seedling holder. At a water content of 10%, a loamy soil (Haplic Phaeozem) was sieved stepwise to < 4 , < 2 and < 1 mm and fertilised following the protocol of Vetterlein *et al.* (2021). Each microcosm was filled with the loamy soil at a

dry bulk density of 1.2 g cm^{-3} . Plants were grown for 14 d in a climate chamber at a temperature of 22°C during day (12 h) and 18°C during night (12 h). Relative humidity was kept constant at 65%. Every day, the microcosms were rewatered to an initial water content of $22 \text{ cm}^3 \text{ cm}^{-3}$. A comprehensive summary of soil and growth conditions is available in Vetterlein *et al.* (2021). As the image contrast between roots/hairs and pore space highly depends on the degree of soil saturation, we stopped watering the plants 2 d before image acquisition in order to drain macropores. Plants were transported alive to the X02DA TOMCAT beamline of the Swiss Light Source synchrotron. To increase the sample size and range of soil matric potentials, we carried out a follow-up experiment at the PSICHE beamline at Synchrotron SOLEIL, France. Sample size (130 mm length, 4.5 mm inner diameter) and dry bulk density (1.3 g cm^{-3}) were similar. A wide range of soil water conditions was reached by saturating the soil every second day. We stopped watering the plants only 1 d before image acquisition.

Imaging and image processing

Shortly before the scanning procedure, the plastic cylinders were disconnected from the seedling holders by using a razor blade. The cylinders were then sealed with parafilm and scanned individually (scan time: *c.* 5 min). At both beamlines, the X-ray beam energy was tuned to 20 keV and the detection systems allowed for an actual pixel size of $0.65 \times 0.65 \mu\text{m}^2$. A detailed description including the detector systems of both beamlines as well as the applied image reconstruction algorithms is available in Duddek *et al.* (2022).

The collected CT datasets consisting of 2160 images per image stack (Fig. 1) had a physical size of $3.05 \text{ mm} \times 2.28 \text{ mm} \times 1.40 \text{ mm}$ and were processed in AVIZO (Thermo Fisher Scientific, 2020). To reduce computational costs, 16-bit greyscale images were converted to 8-bit images and regions of interest were cropped. Although we aimed for cubic image stacks (same dimensions in each direction), the *x* and *y* dimensions of individual samples were slightly adjusted to avoid cutting off visible root hairs. The sample that deviated the most from a cubic shape had the dimensions $1.79 \text{ mm} \times 1.28 \text{ mm} \times 1.40 \text{ mm}$. We applied a nonlocal means filter to the data collected at SOLEIL. This was not needed for the TOMCAT data due to its higher signal : noise ratio. We then applied an unsharp masking filter, before utilising a watershed transformation to segment the data.

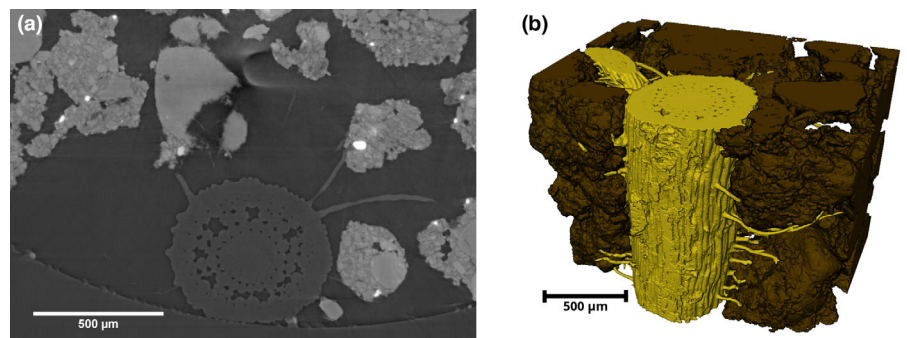


Fig. 1 Reconstructed and segmented images of a maize (*Zea mays*) root growing in a loamy soil (adapted from Duddek *et al.*, 2022). (a) 2D slice showing a root and its hairs surrounded by air-filled macropores and soil aggregates (Bar, 500 μm). (b) 3D rendering showing a root segment as well as root hairs (in yellow) and the soil matrix (in brown; Bar, 500 μm).

The watershed transformation was applied multiple times on each sample to iteratively improve the output of the segmentation. Note that this approach only allowed us to segment turgid root hairs. The resulting label fields were composed of air-filled soil pores, soil matrix and root domains. We assigned micropores to the soil matrix by applying morphological closing (r_{sphere} : 12 px) and the fill holes algorithm in AVIZO. Morphological opening allowed to separate roots and hairs digitally and assign them individual labels. Furthermore, we generated root endodermis (15 μm thickness) and stele areas by morphologically eroding root cylinders and again assigned both domains separate labels. The radii of the structuring element (sphere) were adjusted based on the visible interface between root cortex and stele in the images. Finally, we extracted and labelled the outer bound of the region of interest. The label field resulting from this workflow was the basis for both generating a finite element mesh and quantifying various soil and root-related measures. It comprised of the following domains: outer bound of the region of interest, air-filled macropores, soil-micropore region (more specifically solid soil phase + micropores; in the

remainder of the text, this region is referred to as the soil matrix), root hairs, root cylinder, endodermis and stele (Fig. 2c). The comprehensive flowchart of the image processing procedure is available in Supporting Information Fig. S1. We quantified the root surface area, the number of hairs and the volume of both the soil matrix and air-filled macropores within the image stacks by conducting a label analysis. Furthermore, we calculated the contact area between soil matrix and roots/root hairs by utilising the label interface module in AVIZO. These measures allowed us to calculate the fraction of epidermis and hairs in contact with soil, the root hair density and the soil macro porosity. We then computed the root hair length by applying a geodesic distance transformation and extracting the maximum distance for each hair individually.

Mesh generation

By applying a marching cubes algorithm (Hege *et al.*, 1997) to the described label field in AVIZO, a surface mesh was generated for each sample. Those surface meshes were simplified by setting

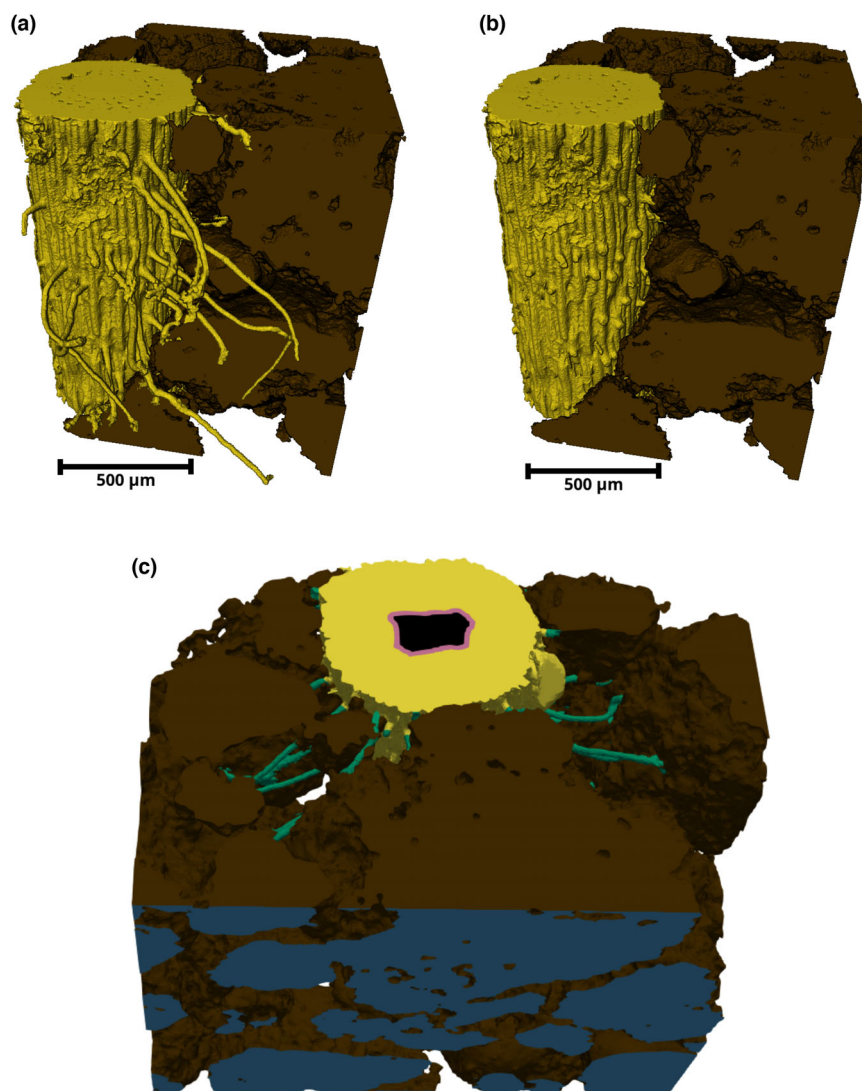


Fig. 2 3D rendering of exemplary root segment (a) before and (b) after removing root hairs by applying morphological operations (Bar, 500 μm). (c) Illustration of geometry patches: inlet in blue, soil matrix in brown, hairs in green, root in yellow, endodermis in pink and outlet in black.

the maximum triangle distance to 20 μm . Subsequently, the number of vertices was halved by applying the remesh surface module. We extracted the following subdomains of the surface mesh as stl files: interface between outer bound of the region of interest and soil matrix (we refer to this patch as inlet), soil matrix, root hairs, root cylinder, root endodermis, interface between endodermis and stele (we refer to this patch as outlet). For each sample, the described workflow was applied a second time after removing the root hair domain from the label field. This approach allowed us to compare the water uptake of each sample with its hairless twin. Based on the previously extracted stl files, we obtained a volumetric polyhedral mesh using SNAPPY-HEXMESH, an inbuilt meshing utility in OPENFOAM (Jasak, 2009). Grid quality was inspected using the CHECKMESH utility. The generated meshes consisted of 20 ± 7 million cells and exhibited a maximum aspect ratio of 8.6 ± 2.22 and an average nonorthogonality of 5.96 ± 0.09 . The flowchart of the mesh generation is available in Fig. S2. We additionally conducted a grid convergence study (Methods S1) to ensure that our results are independent of the mesh resolution.

Mathematical model

To compute root water uptake of maize root segments in partially saturated loamy soil, we simulated the propagation of water potential gradients in the root–soil continuum. Developing an image-based 3D model allowed to explicitly take rhizosphere features, such as root hairs, root–soil matrix contact and aggregate structure into account. To assess the efficacy of root hairs in water uptake, we conducted simulations on a set of six maize root segments of *c.* 1.4 mm length (Fig. 5) and then repeated them after digitally removing the root hairs (Fig. 2a,b). The considered root segments were static (nongrowing), and we only included turgid root hairs in the geometries. As macropores of the utilised soil were drained even in the wettest scenario (Fig. 3a), we neglected the soil macropores and only considered the soil matrix as a flow domain in our simulations. Fig. 3 shows that these micropores were, depending on the soil matric potential, (partially) water or

air-filled. The fact that smaller micropores appeared air-filled in drier soil conditions shows that these pores were hydraulically connected and could be drained. Nevertheless, the minimum pore size that we could resolve was limited by the theoretical spatial resolution of 1.3 μm ($2 \times$ actual pixel size). As the greyscale of smaller pores reflected a mixed phase (solid, liquid and gaseous phase), we treated the soil matrix in an effective way by applying the Richardson–Richards equation (Richardson, 1922; Richards, 1931). We therefore estimated the hydraulic parameters of the soil matrix based on the water retention curve (Vetterlein *et al.*, 2021), determined using the bimodal model of Durner (1994). Note that excluding macropores from the simulations did not affect the generality of our findings, because in conditions when the macropores contribute to the water flow, hairs would be irrelevant. The swelling and shrinking behaviour of micropores and of the root cortex due to soil drying and rewetting cycles were neglected in our model. Furthermore, we neglected the influence of root hairs on rhizosphere structure formation, such as their effect on soil porosity and pore connectivity (Koebernick *et al.*, 2017; Hallett *et al.*, 2022).

Mathematically, our model is described as follows:

Let $\Omega \subset \mathbb{R}^3$ represent the spatial domain obtained from the CT images (Fig. 2c) and $[0, T]$ the time interval until steady state was reached. The boundary of the domain is denoted as $\partial\Omega$ and split into Dirichlet ($\Gamma_D = \Gamma_{D_1} \cup \Gamma_{D_2}$) (outlet (black) and inlet (blue) boundaries in Fig. 2c) and von Neumann (Γ_N) boundary (rest of the domain boundary depicted in Fig. 2c), with $\partial\Omega = \Gamma_D \cup \Gamma_N$.

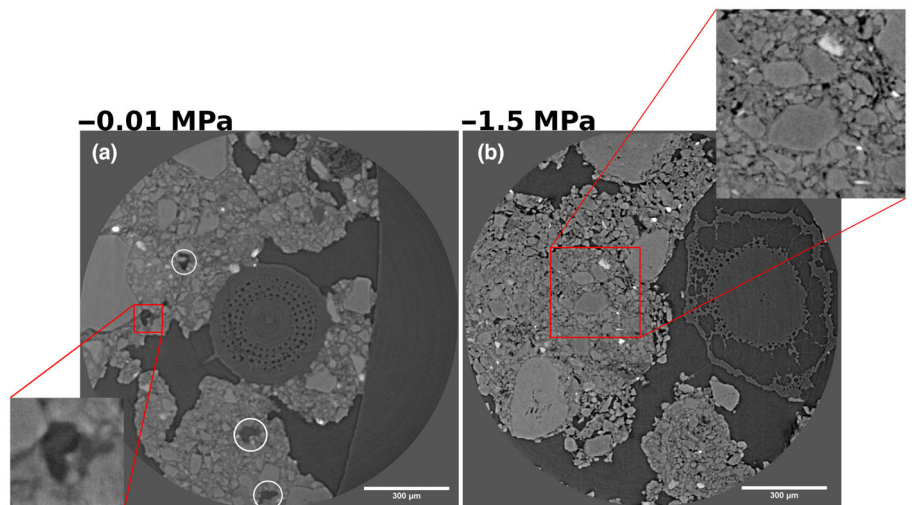
The head-based Richardson–Richards equation is formulated as follows:

$$\frac{d\theta}{dt} = C(h) \frac{dh}{dt} = \nabla \cdot (K(h) \cdot \nabla(h + z)) \quad \text{in } \Omega \times [0, T]$$

Eqn 1

where θ ($\text{m}^3 \text{m}^{-3}$) denotes the volumetric water content, C (m^{-1}) the specific moisture capacity, h (m) the matric head, t (s) the time, $K(h)$ (m s^{-1}) the unsaturated hydraulic

Fig. 3 Reconstructed 2D images showing root (*Zea mays*) and soil domains at different soil matric potentials. (a) Sample scanned at the wettest soil condition considered in our simulations (-0.01 MPa). While the macropores were air-filled, the soil matrix was almost saturated. The two lower circles highlight saturated micropores, while the upper left circle shows an air-filled micropore. The red square highlights a partially saturated micropore with the meniscus visible at the liquid–gas interface in the enlarged image (Bar, 300 μm). (b) Sample scanned at a soil matric potential of -1.5 MPa. A significant number of drained micropores are visible in the enlarged image (Bar, 300 μm).



conductivity, ∇ (m^{-1}) the nabla-operator and z (m) the elevation above a vertical datum.

Throughout the rest of the manuscript, we convert matric potential from energy per unit weight (matric head (m)) into energy per unit volume (matric suction (MPa)) using the simplified relation:

$$-100 \text{ m} \approx -1 \text{ MPa} \quad \text{Eqn 2}$$

We assigned a constant matric potential of -1.5 MPa at the outlet boundary (inner surface of endodermis) Γ_{D_1} (coloured black in Fig. 2c):

$$h_{\text{out}} = -1.5 \text{ MPa} \text{ on } \Gamma_{D_1} \subseteq \partial\Omega \quad \text{Eqn 3}$$

A series of simulations were performed, differing in the matric potential at the inlet (outer boundary of the domain; coloured blue in Fig. 2c). The following set of inlet (Γ_{D_2}) boundary conditions was imposed:

$$h_{\text{in}} \in \{(-1.26, -1.00, -0.32, -0.10, -0.03, -0.01) \text{ MPa}\} \\ \text{on } \Gamma_{D_2} \subseteq \partial\Omega \quad \text{Eqn 4}$$

The choice of $h = -0.01$ MPa as wettest simulation scenario is justified by the fact that macropores of the considered substrate were drained at the corresponding soil matric potential (Fig. 3). Additionally, in wetter conditions the soil is much more conductive than the roots and the effect of hairs becomes negligible. Consequently, excluding soil macropores from the flow domain in our model is valid for the selected set of matric potentials.

As for the rest of the boundary, we assigned a zero flux condition ensuring that water is not leaving the soil matrix or root domains.

$$\nabla h \cdot \mathbf{n} = 0 \text{ on } \Gamma_N \subseteq \partial\Omega \quad \text{Eqn 5}$$

where \mathbf{n} denotes the outward unit normal vector to the surface. As initial condition, we assigned a constant matric potential h_0 to the flow domain.

$$h = h_0 \text{ at } t = 0 \quad \text{Eqn 6}$$

which we adjusted according to the inlet boundary condition of each scenario.

Table 1 Parameterisation of the model according to Mualem (1976) and van Genuchten (1980).

| Parameter | Description | Unit | Soil matrix | Root cortex/hairs | Root endodermis |
|------------|---------------------------------|-------------------------------|----------------------|-----------------------|-----------------------|
| θ_s | Sat. water content | $\text{cm}^3 \text{ cm}^{-3}$ | 0.37 | 0.9 | 0.9 |
| θ_r | Residual water content | $\text{cm}^3 \text{ cm}^{-3}$ | 5.5×10^{-3} | 0 | 0 |
| n | Shape parameter | – | 1.334 | 1.334 | 1.334 |
| α | ~ Inverse of air entry pressure | cm^{-1} | 0.0137 | 1×10^{-20} | 1×10^{-20} |
| K_s | Sat. hydraulic conductivity | cm d^{-1} | 335 | 5.18×10^{-4} | 4.32×10^{-5} |
| τ | Tortuosity factor | – | 0.5 | 0.5 | 0.5 |

Parameters are given for the soil matrix as well as for the root domains (*Zea mays*).

Parameterisation

We parameterised the soil matrix based on the Mualem–van Genuchten model (Mualem, 1976; van Genuchten, 1980). Soil hydraulic parameters of the used soil texture are available in Vetterlein *et al.* (2021). These parameters are based on the Durner bimodal model (Durner, 1994), which constitutes a linear superposition of two subcurves representing a bimodal pore-size distribution. Hence, the hydraulic properties of both the macro and micropore regions are included in this parameter set. As we were only considering water flow within the soil matrix, we used the parameters of the micropore subcurve. We estimated the porosity of the soil matrix ϕ_{matrix} as:

$$\phi_{\text{matrix}} = \frac{\phi_{\text{tot}} - \omega_1}{\omega_2} \quad \text{Eqn 7}$$

where ϕ_{tot} is the total soil porosity and ω_1 and ω_2 are the volumetric fractions of the macro- and micropore regions of the soil, respectively. The full set of soil matrix parameters can be found in Table 1.

The parameterisation of the root consisting of hair, root cortex and endodermis domains was based on noninvasive water flux measurements at the cellular scale (Zarebanadkouki *et al.*, 2019). The authors calculated radial water fluxes in both apoplastic and cell-to-cell pathways based on fast neutron tomographies of lupine root systems in combination with inverse modelling. We estimated the hydraulic conductivity of the root endodermis based on its hydraulic permeability $L_{p,\text{Endo}}$ as:

$$K_{\text{Endo}} = L_{p,\text{Endo}} \cdot d_{\text{Endo}} \quad \text{Eqn 8}$$

where d_{Endo} represents the thickness of the endodermis (15 μm in our study). We further estimated the hydraulic conductivity of the root cortex analogously to a circuit of resistors considering the apoplastic and protoplasmic pathways in parallel, weighted by their volumetric contribution to the overall radial water flow. Consequently, the effective hydraulic conductivity of the root cortex was estimated as follows:

$$K_{\text{root}} = K_{\text{apoplast}} \cdot \frac{V_{\text{apoplast}}}{V_{\text{tot}}} + K_{\text{cell-to-cell}} \cdot \frac{V_{\text{cell-to-cell}}}{V_{\text{tot}}} \quad \text{Eqn 9}$$

We assumed identical hydraulic conductivities for both the root cortex and root hairs and, while neglecting film flow, we

considered water absorption along the entire hair surface. The resulting van Genuchten parameters are presented in Table 1.

Additionally, we took drought stress-induced root hair shrinkage into account by presuming a decline of hydraulic conductivity as hairs shrunk. Due to the high variability of root hair shrinkage in response to successive soil drying (Duddek *et al.*, 2022), we considered two contrasting scenarios that enveloped the entire hair shrinkage dataset (Fig. 4a). We fitted the relation between soil matric potential and root hair turgidity using the van Genuchten function (van Genuchten, 1980). This yielded two root hair turgor loss curves – an analogue of a water retention curve for root hairs – one representing an early and the other one a late onset of hair shrinkage in terms of soil matric potential (Fig. 4a). Assigning the gained van Genuchten parameters to the root hair domain allowed us to implement root hair shrinkage in an effective way. Nevertheless, it still needs to be studied if and to what extent hairs conduct water after shrinkage.

To determine the effect of root hair shrinkage on water uptake, we adjusted the set of inlet boundary conditions stated in Eqn 4. We set the minimum matric potential at the inlet according to the potential at which root hairs started to exhibit a positive effect on water uptake (-0.1 MPa) and decreased the step size as:

$$h_{in} \in \{(-10^{0.1}, -10^0, -10^{-0.1}, -10^{-0.2}, \dots, -10^{-1}) \text{ MPa}\} \text{ on } \Gamma_{D_2} \subseteq \partial\Omega \quad \text{Eqn 10}$$

The equations were solved in OPENFOAM (Open Source Field Operation and Manipulation, v.4.1), a finite volume-based C++ library for CFD applications (Jasak, 2009). In particular, we used a modified version of the RICHARDSFOAM2-SOLVER (Orgogozo *et al.*, 2014) which allowed for adaptive time stepping. The backward Euler scheme was selected for time stepping, Gauss linear as gradient and Gauss harmonic corrected as Laplacian scheme.

Parallellised numerical simulations were performed on 125 cores (250 GB memory) of the Euler cluster operated by the High Performance Computing group at ETH Zürich.

Postprocessing

Postprocessing including the calculation of the volumetric flow rate through the endodermis was conducted in PARAVIEW (v.5.5.2; Ahrens *et al.*, 2005). For this purpose, we calculated the magnitude of the flow field and integrated over the outlet domain (inner surface of endodermis). The efficacy of hairs on root water uptake was estimated as fraction of increase in water uptake between the flow rate of hairy and hairless cases:

$$\frac{\Delta Q}{Q_{\text{hairless}}} = \frac{Q_{\text{hairy}} - Q_{\text{hairless}}}{Q_{\text{hairless}}} \quad \text{Eqn 11}$$

Statistics

The sample size of our study corresponded to six image-based samples. These samples varied in soil macroporosity both at the root–soil interface and in the bulk soil, root hair length and density. The dependent variable was $\Delta Q/Q_{\text{hairless}}$ (Eqn 11) representing the fraction of increase in root water uptake due to root hairs. The random components in these samples were the arrangement and shape of soil aggregates and the spatial distribution of root hairs. We compared the arithmetic means of the computed uptake rates of the hairy and hairless root segments statistically by conducting a paired two-sample *t*-test. To determine the governing variable that explained the highest fraction of the variance in root water uptake, a linear regression was conducted. Significance level was chosen as 0.05. All statistical measures were calculated in RSTUDIO (v.2022.02.3; RStudio Team, 2022).

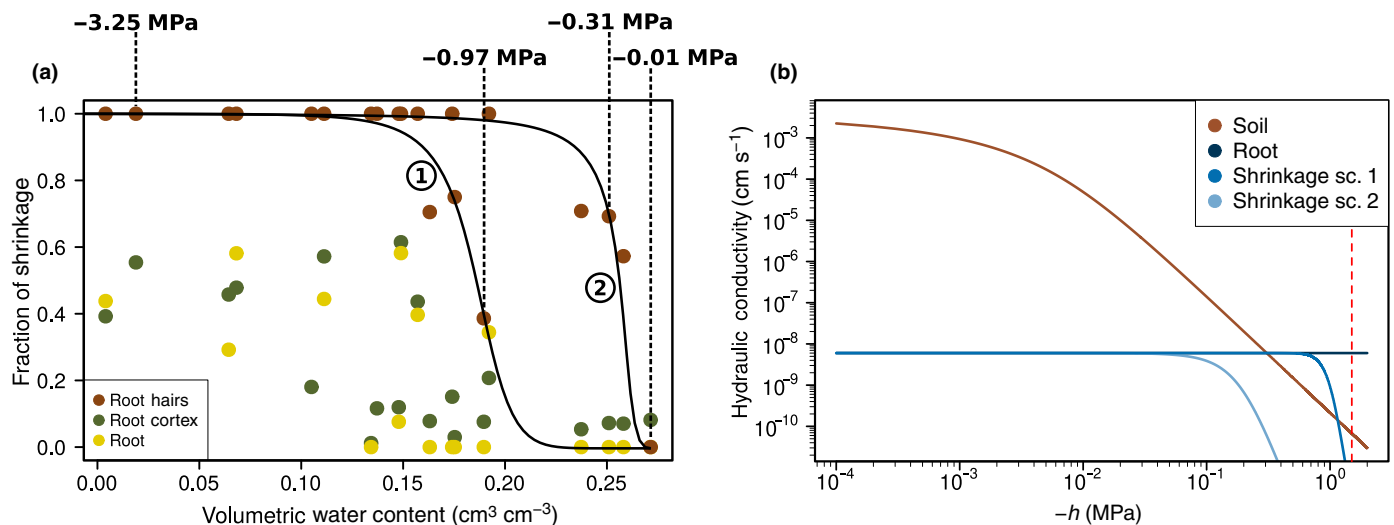


Fig. 4 Model parameterisation. (a) Root and root hair shrinkage (*Zea mays*) in relation to progressive soil drying. Turgor loss curves of root hairs were fitted using the van Genuchten function. Figure adapted from Duddek *et al.* (2022). (b) Hydraulic conductivity curves of the following spatial domains: soil matrix, root cortex + hairs. Additionally, hydraulic conductivity curves for the two considered shrinkage scenarios are presented. Dashed red line indicates outlet boundary condition ($h_{\text{out}} = -1.5$ MPa).

Results

The mean root surface area of the samples was $3.5 \pm 0.6 \text{ mm}^2$ and $22 \pm 13\%$ of the root epidermis was in contact to soil matrix. Mean root hair length was $0.19 \pm 0.05 \text{ mm}$ with $37 \pm 12\%$ hair surface in contact to soil particles. Root hair density (number of hairs per mm of root length) was determined as $50 \pm 20 \text{ mm}^{-1}$. Note that these results are based solely on turgid root hairs. We quantified the soil macroporosity both at the root–soil interface ($0.8 \pm 0.1 \text{ cm}^3 \text{ cm}^{-3}$) and within the overall sample volumes ($0.4 \pm 0.1 \text{ cm}^3 \text{ cm}^{-3}$) and found the latter to be significantly lower ($P < 0.002$). Fig. 1 illustrates an exemplary 2D slice of the obtained CT data and a 3D rendering of the same sample. Fig. 5 shows the entire set of six root segments our study is based on. Steady-state solutions for each geometry and the corresponding scenarios listed in Eqn 4 were computed. Fig. 6(a–d) shows examples of the obtained solutions illustrating the steady-state water potential distribution within the image-based geometry with and without hairs. We quantified the average radial distribution of soil matric potential (Fig. 7) in the immediate vicinity of a root in dry soil conditions ($h_{\text{in}} = -1.26 \text{ MPa}$). Particularly at the root–soil interface, matric potential gradients were larger in the hairless geometry (Fig. 7) compared with the hairy case. The latter represented a more homogeneous water extraction from the soil, which resulted in a higher volumetric uptake rate compared with the hairless root segment. We compared the volumetric flow rates through hairy and hairless root segments in order to estimate the hair-induced increase in water uptake. Our model revealed that, under dry soil conditions ($h_{\text{in}} < -0.1 \text{ MPa}$), water uptake of hairy root segments was substantially bigger than for nonhairy cases (Fig. 8a). Significance of this result was confirmed by a paired *t*-test ($P < 0.013$). In the driest scenario considered in this study ($h_{\text{in}} = -1.26 \text{ MPa}$), root water uptake increased by $24 \pm 18\%$ due to the effect of root hairs. 86% ($R^2 = 0.865$, $P = 0.007$) of the variance in root water uptake was explained by the root hair-induced increase in root–soil contact. The effect of root hair shrinkage was assessed by comparing two shrinkage scenarios: one representing an early and one a later onset of hair shrinkage in terms of soil matric

potential (Fig. 4a,b; Table 2). The simulations were based on the sample in which the hairs had the greatest impact on water absorption. The efficacy of root hairs in water uptake was strongly reduced due to shrinkage (Fig. 8b). Considering shrinkage scenario 2 (Fig. 4a, early onset of hair shrinkage in terms of soil matric potential), the positive effect of root hairs vanished. The reason for this is illustrated in Fig. 4(b): in shrinkage scenario 2, the hydraulic conductivity of the soil matrix was higher than that of hairs in the entire interval of simulated water potentials. Hence, at any soil matric potential in our simulations, the soil matrix was more conductive than root hairs. However, for shrinkage scenario 1 (Fig. 4a), our model predicted a positive impact of hairs between $h_{\text{in}} = -1 \text{ MPa}$ and $h_{\text{in}} = -0.1 \text{ MPa}$. This is the interval where the hydraulic conductivity of the hairs was larger than that of the soil matrix (Fig. 4b). At $h_{\text{in}} = -1 \text{ MPa}$, the root hair hydraulic conductivity dropped dramatically due to shrinkage, which eliminated the effect of hairs.

To determine the sensitivity of our results to the ratio of hydraulic conductivities of root (hair) vs soil domains, we performed additional simulations with adjusted van Genuchten parameters for the root (hair) domains (Table S1). Ultimately, the effect of root hairs on root water uptake depended on this ratio (Fig. S3), but the implications of our model were robust to changes in this ratio as long as the hydraulic conductivity of the hairs exceeded that of the soil matrix at water potential higher than -1 MPa (Fig. 4b). To estimate the spatial discretisation error of our simulations, we conducted a grid convergence study (Tables S2, S3), which indicated that our simulations were robust to grid refinement.

Discussion

According to our model, the efficacy of root hairs in water uptake is governed by the hair-induced increase in root–soil contact (Fig. 9). Note that this parameter is not only related to root (hair) traits (i.e. root hair length and density) but also to soil parameters. It depends on the contact area between soil and both root epidermis and hairs and thus relates to the soil macroporosity both at the root–soil interface and within the bulk soil.

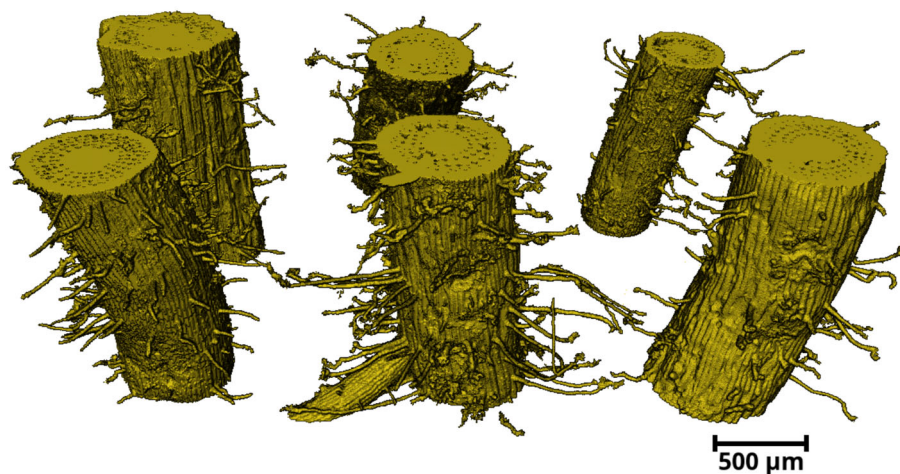


Fig. 5 Set of root segments (*Zea mays*) used in our simulations (Bar, $500 \mu\text{m}$).

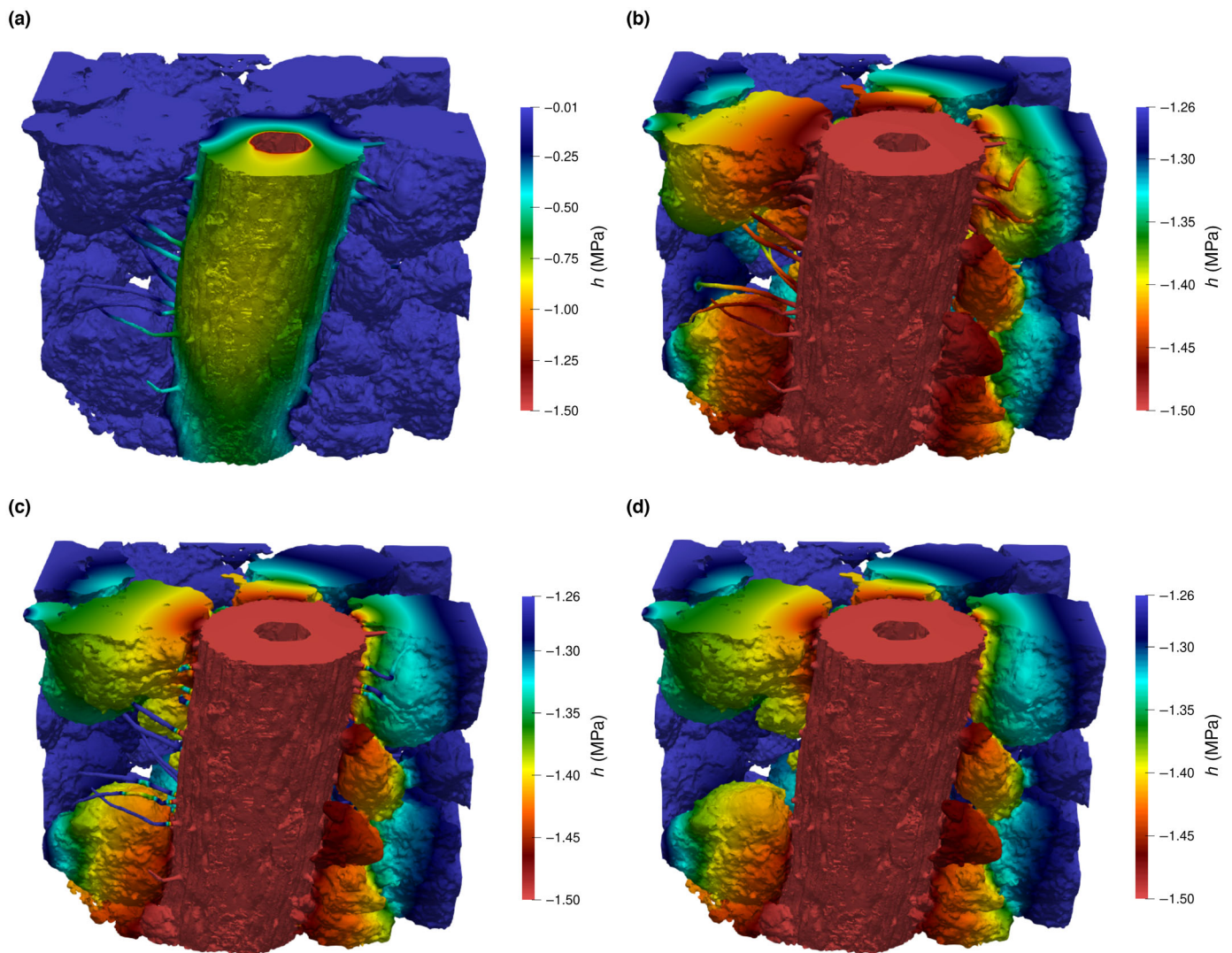


Fig. 6 Steady-state modelling results illustrating water potential distribution within the root–soil continuum. (a) Hairy root segment in wet soil conditions ($h_{in} = -0.01$ MPa). Gradients in water potential visible in the root domain suggest that not the soil matrix but the root limits water flow. (b) Hairy root segment in dry soil conditions ($h_{in} = -1.26$ MPa). Gradients in matric potential occur in the soil matrix, which constitutes the limiting domain for water flow in this example. (c) Hairy root segment ($h_{in} = -1.26$ MPa) with root hairs not active in water uptake due to shrinkage (shrinkage scenario 2). (d) Hairless root segment in dry soil conditions ($h_{in} = -1.26$ MPa). In comparison with (b), less dispersion in water potential is visible around the root, indicating that the corresponding gradients are larger. The distribution of soil matric potential is similar in the hairless and shrinkage cases (see c, d).

Furthermore, we demonstrated that root hairs bear the potential to facilitate root water uptake at low matric potentials (< -0.1 MPa, Fig. 8a) when water fluxes in soil are limited. Root hairs partially divert water flow from within the soil into the hairs, which leads to a more homogeneous water extraction throughout the rhizosphere. This means that within the rhizosphere, the sink term is distributed over a range of radial distances from the root–soil interface the water flux and hence the hydraulic gradient at the root–soil interface is reduced. We could demonstrate that indeed, at the root–soil interface, the gradient in soil matric potential was considerably larger in the hairless case (Fig. 7), which translates into a bigger drop in unsaturated hydraulic conductivity. These findings are in agreement with the conceptual model of Carminati *et al.* (2017).

Although our model predicts that root hairs potentially facilitate root water uptake under dry soil conditions, root hair shrinkage in maize is initiated at relatively high soil matric potentials (Duddek *et al.*, 2022). Root hair turgidity may be susceptible to both hair age and water stress, meaning that hairs of different ages may exhibit distinct shrinkage behaviours. Evidence for this has been reported by Xiao *et al.* (2020), who found that relatively old (19 d) cotton root hairs collapsed at presumably mild water stress (45% soil rel. water content, no translation to matric potential available). Taking this into consideration, we simulated the two shrinkage scenarios based on the dataset of Duddek *et al.* (2022) (Fig. 4a). Depending on the turgor loss curve, the effect of hairs is substantially reduced. For scenario 2 (early onset of hair shrinkage in terms of soil matric potential) which may

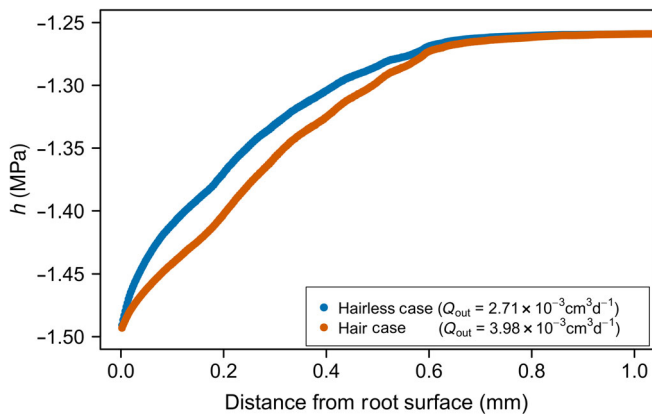


Fig. 7 Average soil matric potential at steady state in relation to the distance from the root surface based on an exemplary sample with $h_{in} = -1.26$ MPa. Particularly at the root–soil interface, gradients in soil matric potential are larger in the hairless scenario. Additionally, the uptake rates (volumetric flow rates Q through the root) for both scenarios are presented.

apply to relatively old root hairs, the effect of hairs was entirely eliminated. However, in scenario 1, which was based on a late onset of hair shrinkage in terms of soil matric potential and could apply to relatively young root hairs, the effect of hairs was still notable between -1 and -0.1 MPa. This suggests that root hairs have a positive effect on root water uptake in a relatively narrow range in soil water potential, which ultimately depends on the susceptibility of root hairs to water stress and therefore presumably on root hair age. Nevertheless, the extent to which the hydraulic conductivity of hairs decreases after shrinkage still needs to be investigated. Note that the soil matric potential range of -1 to -0.1 MPa coincides with the water potential range in which transpiration rate decreases due to stomatal closure (Koehler *et al.*, 2022). The authors carried out a soil column

experiment using the same maize genotype grown in the same soil texture as in our experiment and measured the relationship between soil water potential and transpiration rate.

Neglecting the differing hydraulic parameters between bulk soil and rhizosphere, Segal *et al.* (2008) found limited mass flow within the inter-root hair domain caused by negligible soil matric potential gradients within this region. They concluded that root hairs did not facilitate water uptake by increasing the root surface area. However, our image-based model, which inherently includes rhizosphere features such as increased porosity at the root–soil interface relative to the bulk soil (Helliwell *et al.*, 2017; Koebernick *et al.*, 2019; Landl *et al.*, 2021), contradicts the findings of Segal *et al.* (2008). As shown by Landl *et al.* (2021), the enhanced porosity at the root–soil interface reduced the soil water retention and hence lead to a reduced water uptake through the root cylinder. The gaps that appeared between the root cylinder and soil matrix formed capillary barriers for water flow, which could be bridged by root hairs. It is worth noting that there is also evidence of decreasing porosity at the root–soil interface (Bruand *et al.*, 1996; Young, 1998; Aravena *et al.*, 2011, 2014), which would result in an elevated root water uptake through the root cylinder and a lower importance of root hairs. Lucas *et al.* (2019) proposed that the porosity around roots can be both elevated and reduced, depending on the initial soil density. Nevertheless, the discrepancy between our study and the one of Segal *et al.* (2008) emphasises the relevance of incorporating rhizosphere traits as effective parameters in upscaled models.

By comparing root hair defective mutants with the corresponding wild-types, several authors reported a positive impact of hairs (Carminati *et al.*, 2017; Marin *et al.*, 2021), while others could not find marked differences between genotypes (Suzuki *et al.*, 2003; Dodd *et al.*, 2016; Cai *et al.*, 2021; Jorda *et al.*, 2022). It is worth noting that even for the same species, namely barley, experimental results were contradictory (Dodd *et al.*,

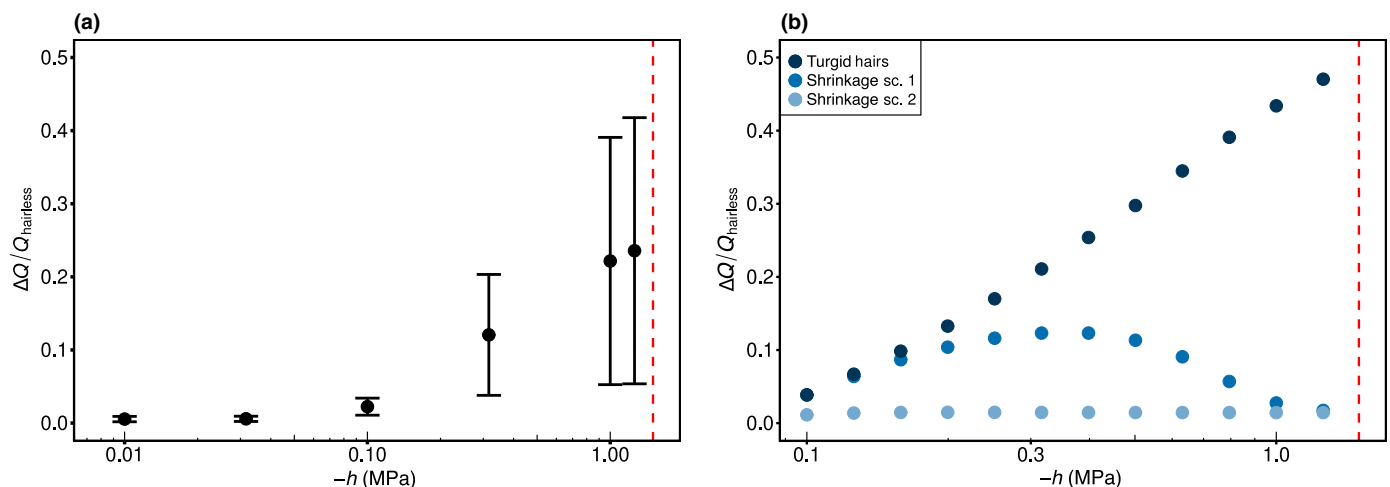


Fig. 8 Postprocessing results. (a) Fraction of increase in root water uptake due to hairs in relation to the matric potential h ($\Delta Q = Q_{hairly} - Q_{hairless}$). Plot illustrates arithmetic mean \pm SD of a set of six samples. (b) Effect of root hair shrinkage: The two considered root hair shrinkage scenarios are compared with the case of turgid hairs for the sample that exhibited the largest effect of root hairs on water uptake. While the effect of hairs is eliminated in shrinkage scenario 2, there is still a visible effect between $h_{in} = -1$ MPa and $h_{in} = -0.1$ MPa in shrinkage scenario 1. The red dashed lines refer to outlet boundary condition ($h_{out} = -1.5$ MPa).

Table 2 Parameterisation of the two considered root hair shrinkage scenarios.

| Parameter | Unit | Root hairs | |
|------------|------------------------------|------------------------|-----------------------|
| | | Shrinkage scenario 1 | Shrinkage scenario 2 |
| θ_s | $\text{cm}^3 \text{cm}^{-3}$ | 1 | 1 |
| θ_r | $\text{cm}^3 \text{cm}^{-3}$ | 0 | 0 |
| n | – | 8.311 | 3.389 |
| α | cm^{-1} | 9.945×10^{-5} | 4.97×10^{-4} |
| K_s | cm d^{-1} | 5.18×10^{-4} | 5.18×10^{-4} |
| τ | – | 0.5 | 0.5 |

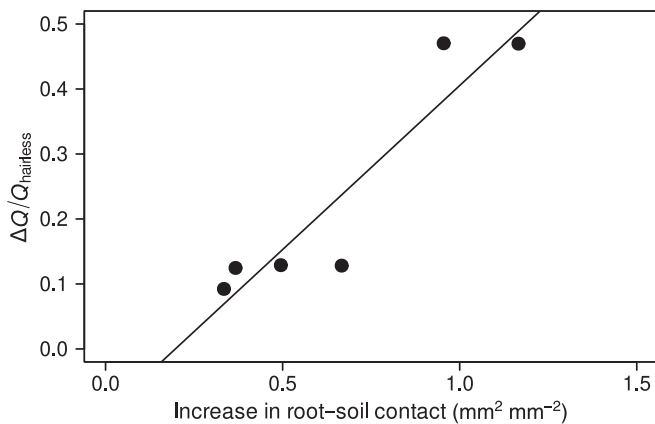


Fig. 9 Correlation between hair-induced increase in root–soil contact and fraction of increase in root water uptake ($h_{in} = -1.26 \text{ MPa}$; $R^2 = 0.86$, $P = 0.007$).

2016; Carminati *et al.*, 2017; Marin *et al.*, 2021). While it has been well recognised that a possible effect of hairs on water uptake will be most pronounced under dry soil conditions (Carminati *et al.*, 2017; Cai *et al.*, 2021; Marin *et al.*, 2021), there is still an ongoing discussion about the lacking effect of hairs in various datasets. The authors mainly focussed on root hair traits (e.g. root hair length and density) as explanatory variables and indeed, root hair lengths between barley and maize differ considerably: in barley, an average length of 0.6 mm was reported (Burak *et al.*, 2021), while we measured a length of $0.2 \pm 0.05 \text{ mm}$ in maize, which is shorter than the result of 0.3 mm reported by Burak *et al.* (2021). Nevertheless, our model suggests that the effect of hairs also depends on soil parameters (e.g. porosity or bulk density). Thus, the role of soil needs to be considered in the aforementioned studies as it potentially explains the contradicting findings.

Instead of comparing a root hair defective mutant with its corresponding wild-type, we applied our model to hairy maize wild-type samples before and after digitally removing their hairs. This allowed us to study the impact of hairs solely focusing on geometrical aspects (e.g. the hair distribution within the soil), hair traits (e.g. hair length and density) and soil parameters (e.g. soil aggregation and macroporosity), while neglecting potential compensation mechanisms of the root hair defective mutant. For instance, Dodd *et al.* (2016) found longer root systems in a barley mutant compared with the wild-type and

Koebnick *et al.* (2017) found a decreased porosity around hairless roots. Jorda *et al.* (2022) reported a larger root : shoot ratio in the maize mutant. While the findings of Koebnick *et al.* (2017) turned out to be insignificant regarding permeability and solute diffusion, Dodd *et al.* (2016) and Jorda *et al.* (2022) speculated that these increased quantities may explain the lack of root hair effect within their studies.

In addition, Jorda *et al.* (2022) emphasised that, in the framework of their field experiment, the root systems of both genotypes were massively ‘oversized’; the active root length in wet soil that would theoretically suffice to cover the entire water demand corresponded to only 10% of the total root length. This may imply that roots continuously grew towards wet soil regions, which could be explained by plant mechanisms known as hydrotropism (Dietrich *et al.*, 2017) and hydropatterning (Bao *et al.*, 2014). In such a scenario, root hairs would indeed play a minor role in water uptake. As our model is limited to the scanned root segments of *c.* 1.4 mm length, these mechanisms are not taken into account. To do that, one would need to consider upscaled models at the root, root system or even field scale.

A less significant role of root hairs is also expected in denser soils, because the root–soil contact would be already enhanced. This might apply to roots reaching dense soil layers in the plough pan or deeper in the subsoil. Additionally, as shown for wheat, root hairs may not even elongate if roots establish a considerable contact with the soil (White & Kirkegaard, 2010). The authors found that root hair density per unit root length dropped exponentially as a function of root–soil contact.

We would like to emphasise that our model was not built for simulating root water uptake of entire roots or root systems. For this purpose, the high level of detail obtained from synchrotron radiation X-ray CT images would not gain further insights. Instead, the computational requirements would be tremendous and by far exceed the available resources. The intention of our model was to rather gain a mechanistic understanding of the effect of root hairs in root water uptake. Furthermore, the extraction of effective rhizosphere parameters at the pore scale can be utilised to parameterise root and root architecture models such as R-SWMS (Javaux *et al.*, 2008).

Limitations of our model include the fact that we have neglected that root hairs can alter the structure of the soil environment and the soil hydrological properties (Hallett *et al.*, 2022). While root hairs have been shown to affect the porosity and connectivity of the (visible) pore space (Koebnick *et al.*, 2017), other studies have suggested that root hairs have no significant effect on pore structure (Koebnick *et al.*, 2018) and water sorptivity (Marin *et al.*, 2021).

We are aware that our experimental approach is prone to artefacts. At the spatial scale of our experiments and images, the heterogeneity of soil packing and hence soil porosity is high and the occurrence of soil layering cannot be ruled out. In addition, high soil porosity tends to occur at the cylinder walls, resulting in favoured growth paths due to gradients in soil mechanical resistance. Furthermore, controlling the water status throughout the rhizosphere, which is difficult in general, becomes even more intricate in the experimental setup we used. This is caused by the

- Aravena JE, Berli M, Ruiz S, Suárez F, Ghezzehei TA, Tyler SW. 2014. Quantifying coupled deformation and water flow in the rhizosphere using X-ray microtomography and numerical simulations. *Plant and Soil* 376: 95–110.
- Bao Y, Aggarwal P, Robbins NE, Sturrock CJ, Thompson MC, Tan HQ, Tham C, Duan L, Rodriguez PL, Vernoux T *et al.* 2014. Plant roots use a patterning mechanism to position lateral root branches toward available water. *Proceedings of the National Academy of Sciences, USA* 111: 9319–9324.
- Bates TR, Lynch JP. 2001. Root hairs confer a competitive advantage under low phosphorus availability. *Plant and Soil* 236: 243–250.
- Brown LK, George TS, Dupuy LX, White PJ. 2013. A conceptual model of root hair ideotypes for future agricultural environments: what combination of traits should be targeted to cope with limited P availability? *Annals of Botany* 112: 317–330.
- Bruand A, Cousin I, Nicoullaud B, Duval O, Bégon JC. 1996. Backscattered electron scanning images of soil porosity for analyzing soil compaction around roots. *Soil Science Society of America Journal* 60: 895–901.
- Burak E, Quinton JN, Dodd IC. 2021. Root hairs are the most important root trait for rhizosheath formation of barley (*Hordeum vulgare*), maize (*Zea mays*) and *Lotus japonicus* (Gifu). *Annals of Botany* 128: 45–57.
- Cai G, Carminati A, Abdalla M, Ahmed MA. 2021. Soil textures rather than root hairs dominate water uptake and soil–plant hydraulics under drought. *Plant Physiology* 187: 858–872.
- Cai G, Vanderborght J, Couvreur V, Mboh CM, Vereecken H. 2018. Parameterization of root water uptake models considering dynamic root distributions and water uptake compensation. *Vadose Zone Journal* 17: 160125.
- Cailloux M. 1972. Metabolism and the absorption of water by root hairs. *Canadian Journal of Botany* 50: 557–573.
- Carminati A, Moradi AB, Vetterlein D, Vontobel P, Lehmann E, Weller U, Vogel H-J, Oswald SE. 2010. Dynamics of soil water content in the rhizosphere. *Plant and Soil* 332: 163–176.
- Carminati A, Passioura JB, Zarebanadkouki M, Ahmed MA, Ryan PR, Watt M, Delhaize E. 2017. Root hairs enable high transpiration rates in drying soils. *New Phytologist* 216: 771–781.
- Couvreur V, Faget M, Lobet G, Javaux M, Chaumont F, Draye X. 2018. Going with the flow: multiscale insights into the composite nature of water transport in roots. *Plant Physiology* 178: 1689–1703.
- Couvreur V, Vanderborght J, Draye X, Javaux M. 2014. Dynamic aspects of soil water availability for isohydric plants: focus on root hydraulic resistances. *Water Resources Research* 50: 8891–8906.
- Daly KR, Keyes SD, Masum S, Roose T. 2016. Image-based modelling of nutrient movement in and around the rhizosphere. *Journal of Experimental Botany* 67: 1059–1070.
- Daly KR, Tracy SR, Crout NM, Mairhofer S, Pridmore TP, Mooney SJ, Roose T. 2018. Quantification of root water uptake in soil using X-ray computed tomography and image-based modelling. *Plant, Cell & Environment* 41: 121–133.
- Dietrich D, Pang L, Kobayashi A, Fozard JA, Boudolf V, Bhosale R, Antoni R, Nguyen T, Hiratsuka S, Fujii N *et al.* 2017. Root hydrotropism is controlled via a cortex-specific growth mechanism. *Nature Plants* 3: 1–8.
- Dodd IC, Diatloff E, Dodd IC, Diatloff E. 2016. Enhanced root growth of the brb (bald root barley) mutant in drying soil allows similar shoot physiological responses to soil water deficit as wild-type plants. *Functional Plant Biology* 43: 199–206.
- Doussan C, Pagès L, Vercambre G. 1998. Modelling of the hydraulic architecture of root systems: an integrated approach to water absorption—model description. *Annals of Botany* 81: 213–223.
- Duddek P, Carminati A, Koebernick N, Ohmann L, Lovric G, Delzon S, Rodriguez-Dominguez CM, King A, Ahmed MA. 2022. The impact of drought-induced root and root hair shrinkage on root–soil contact. *Plant Physiology* 189: 1232–1236.
- Dunbabin VM, McDermott S, Bengough AG. 2006. Upscaling from rhizosphere to whole root system: modelling the effects of phospholipid surfactants on water and nutrient uptake. *Plant and Soil* 283: 57–72.
- Durner W. 1994. Hydraulic conductivity estimation for soils with heterogeneous pore structure. *Water Resources Research* 30: 211–223.
- Gahoonia TS, Nielsen NE. 1997. Variation in root hairs of barley cultivars doubled soil phosphorus uptake. *Euphytica* 98: 177–182.
- Gahoonia TS, Nielsen NE. 2003. Phosphorus (P) uptake and growth of a root hairless barley mutant (bald root barley, brb) and wild type in low- and high-P soils. *Plant, Cell & Environment* 26: 1759–1766.
- Gardner WR. 1960. Dynamic aspects of water availability to plants. *Soil Science* 89: 63–73.
- van Genuchten MT. 1980. A closed-form equation for predicting the hydraulic conductivity of unsaturated soils. *Soil Science Society of America Journal* 44: 892–898.
- Gregory P. 2006. Roots, rhizosphere and soil: the route to a better understanding of soil science? *European Journal of Soil Science* 57: 2–12.
- Haling RE, Brown LK, Bengough AG, Young IM, Hallett PD, White PJ, George TS. 2013. Root hairs improve root penetration, root–soil contact, and phosphorus acquisition in soils of different strength. *Journal of Experimental Botany* 64: 3711–3721.
- Hallett PD, Marin M, Bending GD, George TS, Collins CD, Otten W. 2022. Building soil sustainability from root–soil interface traits. *Trends in Plant Science* 27: 688–698.
- Hege H-C, Stalling D, Seebass M, Zockler M. 1997. A generalized marching cubes algorithm based on non-binary classifications. *ZIB Preprint* SC-97-05.
- Helliwell JR, Sturrock CJ, Mairhofer S, Craigan J, Ashton RW, Miller AJ, Whalley WR, Mooney SJ. 2017. The emergent rhizosphere: imaging the development of the porous architecture at the root–soil interface. *Scientific Reports* 7: 14875.
- Hetrick BAD. 1991. Mycorrhizas and root architecture. *Experientia* 47: 355–362.
- Hinsinger P, Bengough AG, Vetterlein D, Young IM. 2009. Rhizosphere: biophysics, biogeochemistry and ecological relevance. *Plant and Soil* 321: 117–152.
- Jasak H. 2009. OPENFOAM: open source CFD in research and industry. *International Journal of Naval Architecture and Ocean Engineering* 1: 89–94.
- Javaux M, Schröder T, Vanderborght J, Vereecken H. 2008. Use of a three-dimensional detailed modeling approach for predicting root water uptake. *Vadose Zone Journal* 7: 1079–1088.
- Jones H, Tomos AD, Leigh RA, Jones RGW. 1983. Water-relation parameters of epidermal and cortical cells in the primary root of *Triticum aestivum* L. *Planta* 158: 230–236.
- Jorda H, Ahmed MA, Javaux M, Carminati A, Duddek P, Vetterlein D, Vanderborght J. 2022. Field scale plant water relation of maize (*Zea mays*) under drought – impact of root hairs and soil texture. *Plant and Soil* 478: 59–84.
- Keyes S, Daly K, Gostling N, Jones D, Talboys P, Pinzer B, Boardman R, Sinclair I, Marchant A, Roose T. 2013. High resolution synchrotron imaging of wheat root hairs growing in soil and image based modelling of phosphate uptake. *New Phytologist* 198: 1023–1029.
- Koebernick N, Daly KR, Keyes SD, Bengough AG, Brown LK, Cooper LJ, George TS, Hallett PD, Naveed M, Raffan A *et al.* 2019. Imaging microstructure of the barley rhizosphere: particle packing and root hair influences. *New Phytologist* 221: 1878–1889.
- Koebernick N, Daly KR, Keyes SD, George TS, Brown LK, Raffan A, Cooper LJ, Naveed M, Bengough AG, Sinclair I *et al.* 2017. High-resolution synchrotron imaging shows that root hairs influence rhizosphere soil structure formation. *New Phytologist* 216: 124–135.
- Koebernick N, Schlüter S, Blaser SRGA, Vetterlein D. 2018. Root–soil contact dynamics of *Vicia faba* in sand. *Plant and Soil* 431: 417–431.
- Koehler T, Moser DS, Botezatu Á, Murugesan T, Kaliamoorthy S, Zarebanadkouki M, Bienert MD, Bienert GP, Carminati A, Kholová J *et al.* 2022. Going underground: soil hydraulic properties impacting maize responsiveness to water deficit. *Plant and Soil* 478: 43–58.
- Landl M, Phalempin M, Schlüter S, Vetterlein D, Vanderborght J, Kroener E, Schnepf A. 2021. Modeling the impact of rhizosphere bulk density and mucilage gradients on root water uptake. *Frontiers in Agronomy* 3. doi: 10.3389/fragro.2021.622367.
- Lavelle P. 2002. Functional domains in soils. *Ecological Research* 17: 441–450.
- Li T, Lin G, Zhang X, Chen Y, Zhang S, Chen B. 2014. Relative importance of an arbuscular mycorrhizal fungus (*Rhizophagus intraradices*) and root hairs in plant drought tolerance. *Mycorrhiza* 24: 595–602.

- Lucas M, Schlüter S, Vogel H-J, Vetterlein D. 2019. Roots compact the surrounding soil depending on the structures they encounter. *Scientific Reports* 9: 16236.
- Marin M, Feeney DS, Brown LK, Naveed M, Ruiz S, Koebernick N, Bengough AG, Hallett PD, Roose T, Puértolas J *et al.* 2021. Significance of root hairs for plant performance under contrasting field conditions and water deficit. *Annals of Botany* 128: 1–16.
- Mualem Y. 1976. A new model for predicting the hydraulic conductivity of unsaturated porous media. *Water Resources Research* 12: 513–522.
- Nestler J, Keyes SD, Wissuwa M. 2016. Root hair formation in rice (*Oryza sativa* L.) differs between root types and is altered in artificial growth conditions. *Journal of Experimental Botany* 67: 3699–3708.
- Orgogozo L, Renon N, Soulaïne C, Hénon F, Tomer SK, Labat D, Pokrovsky OS, Sekhar M, Ababou R, Quintard M. 2014. An open source massively parallel solver for Richards equation: mechanistic modelling of water fluxes at the watershed scale. *Computer Physics Communications* 185: 3358–3371.
- Passioura J. 1980. The transport of water from soil to shoot in wheat seedlings. *Journal of Experimental Botany* 31: 333–345.
- Richards LA. 1931. Capillary conduction of liquids through porous mediums. *Physics* 1: 318–333.
- Richardson LF. 1922. *Weather prediction by numerical process*. Cambridge, UK: Cambridge University Press.
- Robbins NE, Dinneny JR. 2015. The divining root: moisture-driven responses of roots at the micro- and macro-scale. *Journal of Experimental Botany* 66: 2145–2154.
- Roose T, Keyes SD, Daly KR, Carminati A, Otten W, Vetterlein D, Peth S. 2016. Challenges in imaging and predictive modeling of rhizosphere processes. *Plant and Soil* 407: 9–38.
- RStudio Team. 2022. *RSTUDIO: integrated development environment for R (v.2022.02.3)*. Boston, MA, USA: RStudio. [WWW document] URL <http://www.rstudio.com/> [accessed 4 July 2022].
- Schnepf A, Carminati A, Ahmed MA, Ani M, Benard P, Bentz J, Bonkowski M, Knott M, Diehl D, Duddek P *et al.* 2022. Linking rhizosphere processes across scales: opinion. *Plant and Soil* 478: 5–42.
- Schnepf A, Leitner D, Landl M, Lobet G, Mai TH, Morandage S, Sheng C, Zörner M, Vanderborght J, Vereecken H. 2018. ROOTBOX: a structural–functional modelling framework for root systems. *Annals of Botany* 121: 1033–1053.
- Segal E, Kushnir T, Mualem Y, Shani U. 2008. Water uptake and hydraulics of the root hair rhizosphere. *Vadose Zone Journal* 7: 1027–1034.
- Steudle E, Jeschke W. 1983. Water transport in barley roots: measurements of root pressure and hydraulic conductivity of roots in parallel with turgor and hydraulic conductivity of root cells. *Planta* 158: 237–248.
- Suzuki N, Taketa S, Ichii M. 2003. Morphological and physiological characteristics of a root-hairless mutant in rice (*Oryza sativa* L.). *Plant and Soil* 255: 9–17.
- Thermo Fisher Scientific. 2020. *AVIZO software for materials research: materials characterization and quality control (v.2020.1)*. [WWW document] URL <https://assets.thermofisher.com/TFS-Assets/MSD/brochures/brochure-avizo-software-materials-research.pdf> [accessed 9 November 2021].
- Tisdall J. 1991. Fungal hyphae and structural stability of soil. *Soil Research* 29: 729.
- Vetterlein D, Lippold E, Schreiter S, Phalempin M, Fahrenkamp T, Hochholdinger F, Marcon C, Tarkka M, Obuger E, Ahmed M *et al.* 2021. Experimental platforms for the investigation of spatiotemporal patterns in the rhizosphere – laboratory and field scale. *Journal of Plant Nutrition and Soil Science* 184: 35–50.
- Watt M, Silk WK, Passioura JB. 2006. Rates of root and organism growth, soil conditions, and temporal and spatial development of the rhizosphere. *Annals of Botany* 97: 839–855.
- White RG, Kirkegaard JA. 2010. The distribution and abundance of wheat roots in a dense, structured subsoil – implications for water uptake. *Plant, Cell & Environment* 33: 133–148.
- de Willigen P, Heinen M, van Noordwijk M. 2018. Roots partially in contact with soil: analytical solutions and approximation in models of nutrient and water uptake. *Vadose Zone Journal* 17: 170060.
- Xiao S, Liu L, Zhang Y, Sun H, Zhang K, Bai Z, Dong H, Li C. 2020. Fine root and root hair morphology of cotton under drought stress revealed with RHIZOPOT. *Journal of Agronomy and Crop Science* 206: 679–693.
- Young IM. 1998. Biophysical interactions at the root–soil interface: a review. *The Journal of Agricultural Science* 130: 1–7.
- Zarebanadkouki M, Trtik P, Hayat F, Carminati A, Kaestner A. 2019. Root water uptake and its pathways across the root: quantification at the cellular scale. *Scientific Reports* 9: 12979.
- Zhang C, Simpson RJ, Kim CM, Warthmann N, Delhaize E, Dolan L, Byrne ME, Wu Y, Ryan PR. 2018. Do longer root hairs improve phosphorus uptake? Testing the hypothesis with transgenic *Brachypodium distachyon* lines overexpressing endogenous RSL genes. *New Phytologist* 217: 1654–1666.

Supporting Information

Additional Supporting Information may be found online in the Supporting Information section at the end of the article.

Fig. S1 Flowchart of the image analysis pipeline.

Fig. S2 Flowchart of the mesh generation pipeline.

Fig. S3 Results of the sensitivity analysis.

Methods S1 Theory of the grid convergence study.

Table S1 Hydraulic conductivity parameterisation for sensitivity analysis.

Table S2 Mesh refinement for grid convergence study.

Table S3 Results of the grid convergence study.

Please note: Wiley is not responsible for the content or functionality of any Supporting Information supplied by the authors. Any queries (other than missing material) should be directed to the *New Phytologist* Central Office.